Tetrahedron 67 (2011) 3440–3447

Contents lists available at ScienceDirect

Tetrahedron

journal homepage: www.elsevier.com/locate/tet

Can the conformational flexibility of *cis*-decalins be modulated through intramolecular O–H···O hydrogen bonding? Profiling the molecular and supramolecular attributes of designer *cis*-fused polycyclitols

Goverdhan Mehta *, Saikat Sen, T.H. Suresha Kumara

School of Chemistry, University of Hyderabad, P.O. Central University, Hyderabad 500046, India

ARTICLE INFO

Article history:
Received 10 January 2011
Received in revised form 17 February 2011
Accepted 16 March 2011
Available online 23 March 2011

Keywords:
Conformational analysis
Conformational restriction
Hydrogen bond
Polycyclitols
Self-assembly

ABSTRACT

In order to unravel the modalities of hydrogen bonding in conformationally flexible polycyclitols *vis-à-vis* their conformationally locked siblings, three diastereomeric perhydro-2,3,4a,6,7,8a-naphthalenehexols, all embodying a 4a,8a-dihydroxy-*cis*-decalin framework, have been synthesized via sequential stereocontrolled oxyfunctionalization of 1,4,5,8-tetrahydronaphthalene. Variable temperature NMR studies on the *cis*-fused polycyclitols thus obtained suggest that their inherent conformational flexibility in solution is restrained at ambient temperature owing either to the formation of a stable H-bonded molecular solvate or to the presence of strong intramolecular O–H···O H-bonding. Single crystal X-ray diffraction studies on the three hexols reveal an interesting commonality in their gross molecular packing and a ubiquitous presence of the $R_2^2(10)$ dimer motif—a supramolecular synthon rarely encountered in the crystal structures of conformationally locked and axially-rich hexols.

1. Introduction

For quite some time now, we have been actively involved in probing the modalities of O–H···O hydrogen bonding in specially designed polyhydroxylated *trans*-decalins (conformationally locked polycyclitols) and exploring the possibility of engineering their solid-state self-assemblies.[1,2] These polyhydroxylated entities, fashioned from a prototypical rigid 4a,8a-dihydroxy-*trans*-decalin backbone, have been shown to predictably lock the hydroxyl functionalities into axial-rich conformations so that those in 1,3-syn-diaxial relationship were automatically brought into a favorable geometry to participate in intramolecular O–H···O hydrogen bonding.[3] The deterministic role played by intramolecular O–H···O H-bonding in their supramolecular assemblies and the conformity of the intermolecular O–H···O H-bonding patterns, observed therein, to core concepts of hydrogen bonding in polyols were amply demonstrated in the crystal structures of several diastereomeric 4aα,8aβ-perhydro-2,3,4a,6,7,8a-naphthalenehexols (**1**–**6**) and their acyl derivatives.[1d–h,j,l]

It may be pertinent to recall that the conceptualization of conformationally locked polycyclitols was, from a purely chronological perspective, largely inspired by the syntheses and intriguing yeast

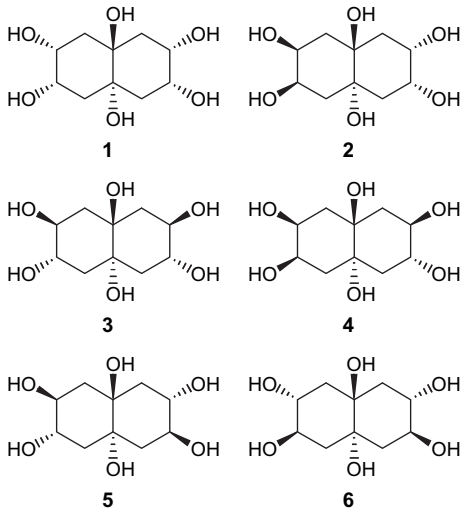

α-glucosidase inhibitory activity of the polycyclitols **7** and **8**, in which the hydroxy functionalities were embedded in a *cis*-hydrindane and *cis*-decalin framework, respectively.[4] Unlike their structural siblings constructed on a *trans*-decalin framework, polyols, such as **7** and **8**, are not destined to exhibit a spatial locking of the hydroxy substituents, and present ideal molecular systems to

* Corresponding author. Tel.: +91 40 23010785; fax: +91 40 23012460; e-mail address: gmsc@uohyd.ernet.in (G. Mehta).

0040-4020/$ – see front matter © 2011 Elsevier Ltd. All rights reserved.
doi:10.1016/j.tet.2011.03.042

study the effect of competing intra- and intermolecular O–H···O hydrogen bonding on the chosen molecular conformation.[5–7]

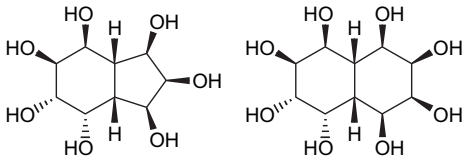

7 (K_i = 84 μM) **8** (K_i = 12 μM)

With the intent of developing a holistic understanding of the supramolecular chemistry of polycyclitols in general, the present endeavor is a retrospective revisitation of polyhydroxylated *cis*-decalins through the representative examples **9**–**11**—all perhydro-2,3,4a,6,7,8a-naphthalenehexols, epimeric with the conformationally locked hexols **1**–**3**. The polyols **9**–**11** were conceptualized to permit a direct comparison of the nuances of their solid-state self-assemblies with that observed in the crystal structures of the polycyclitols **1**–**6**.

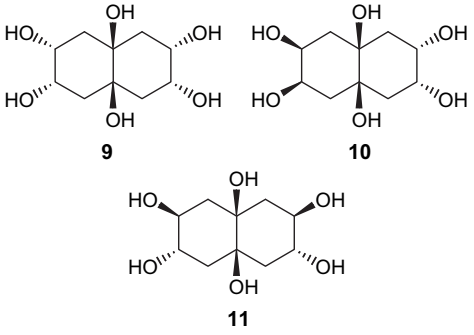

9 **10** **11**

2. Results and discussion

2.1. Synthesis of the diastereomeric hexols 9–11

Synthesis of the hexols **9** and **10** commenced from the acetonide derivative **17**[8] of the diol **16**, which was conveniently prepared from naphthalene following an earlier reported procedure.[2b] Catalytic OsO_4 mediated exhaustive dihydroxylation of **17** furnished an equimolar mixture of two diastereomeric tetrols **18**, which were isolated from the reaction mixture and separated from each other as their bisacetonide derivatives **19** and **20**. Exposure of **19** and **20** to mild acid gave the hexols **9** and **10**, respectively in quantitative yield (Scheme 1).

may be ascribed to the extensive hydration of the more polar concave face (Fig. 2), wherein the intervening water bridges tie down the secondary hydroxyl groups together through an intricate network of O–H···O hydrogen bonding.[9] In case of the hexol **10**, it is the formation of a persistent intramolecular O–H···O H-bond between the 1,3-diaxial hydroxyl groups that prevents a rapid thermal flipping between the two chair conformations of **10** in solution (Fig. 3).[10] Such an effect of hydrogen bonding (intra- and/or inter) on the conformational flexibility of a *cis*-decalin scaffold would be expected to weaken with increasing temperature. Indeed, the ^{13}C spectra, recorded for the hexols **9** and **10** at 343 and 353 K, exhibited the expected three and five carbon resonances, respectively (See Supplementary data for details).

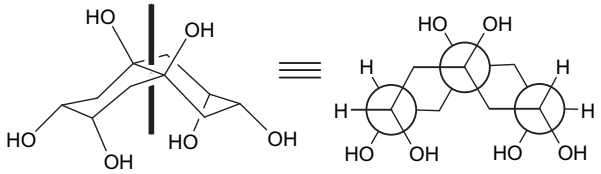

Fig. 1. The twofold symmetry in the hexol **9** will be evident even in the absence of conformational flexibility of the *cis*-decalin scaffold.

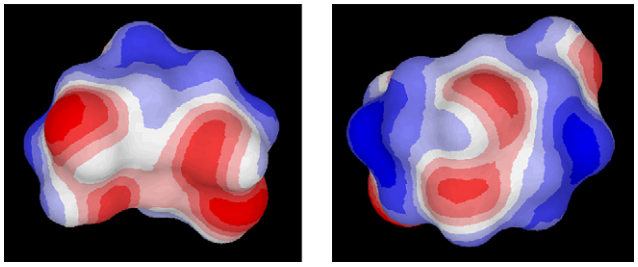

Fig. 2. The molecular electrostatic potential surface of the hexol **9**, showing the predominantly polar concave face (left) as compared to the convex face (right).[11]

The *syn*-diol **22**, obtained by regioselective bromination and subsequent Woodword *cis*-dihydoxylation in **21** (the Birch reduction product of napthalene), formed the starting material for the synthesis of the hexol **11** (Scheme 2).[12] Exhaustive epoxidation of the carbonate derivative **23** of **22** with *m*CPBA furnished a mixture of two diepoxides **24** and **25** in the ratio 7:3. The stereostructure of the major diastereomer **24** was unambiguously assigned by single crystal X-ray diffraction analysis.[13] Mild acid catalyzed ring opening in the mixture of diepoxides, thus obtained, afforded the tetrol **26** as a single diastereomer. Though unexpected, the observed stereo-

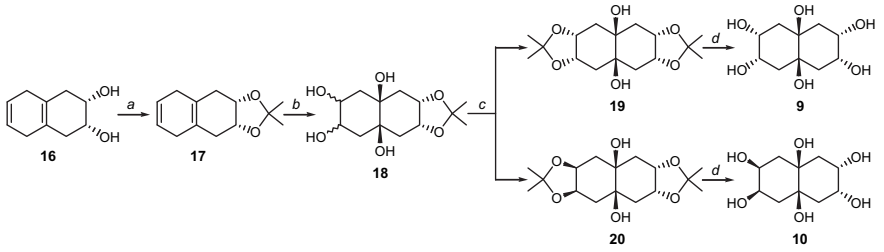

Scheme 1. Reagents and conditions. (a) Amberlyst-15, acetone, MS 4 Å, rt, 1 h, 98%; (b) OsO_4 (5 mol %), NMMO, acetone/water (4:1), rt, 48 h; (c) 2,2-Dimethoxypropane, PPTS, acetone, rt, 2 h, 89% (combined yield over two steps), **19** (44%) and **20** (45%); (d) 10% AcOH (aq), 60 °C, 1 h, quant.

Interestingly, both the C_{2v} symmetric **9** and C_s symmetric **10** displayed a five-line (consistent with the retention of the twofold symmetry, Fig. 1) and a ten-line ^{13}C spectrum, respectively at 298 K, indicating a restraint on the conformational flexibility of the *cis*-decalin framework in the two hexols at ambient temperature. The observed conformational rigidity in the bowl-shaped **9** at 298 K

convergence in the epoxide ring opening of **24** and **25** was quite welcome. A possible, though speculative, rationale for this observation may lie in either a β-face attack of water at position 1 in the intramolecularly hydrogen bonded monoepoxide intermediate **27** or a hydroxy directed α-face attack by hydrogen bonded water at position 2 in **28** (Scheme 3).[14] Base catalyzed carbonate deprotection

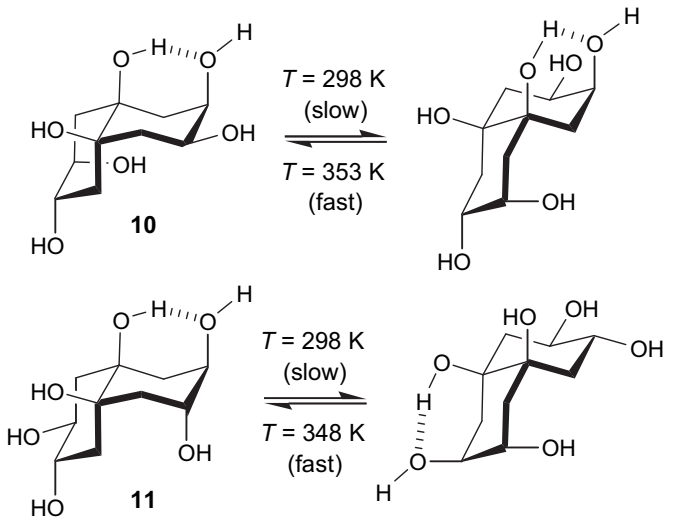

Fig. 3. Restriction of the conformational flexibility of the *cis*-decalin scaffold in the hexols **10** and **11**, brought about by intramolecular O–H···O H-bonding between the 1,3-syndiaxial hydroxy groups.

in **26** yielded the hexol **11** in quantitative yield. For reasons noted for **10**, a ten- and six-line ^{13}C spectrum was also observed for the C_s symmetric hexol **11** at 298 K and 348 K, respectively (Fig. 3).

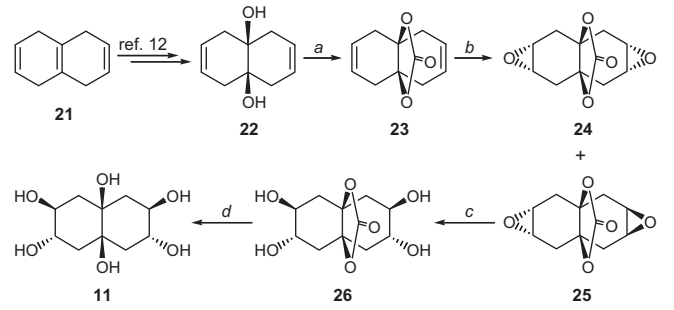

Scheme 2. Reagents and conditions. (a) triphosgene, pyridine, DMAP, DCM, −78 °C to rt, 2 h, 80%; (b) *m*CPBA, DCM, rt, 48 h, 75% (overall yield), **24** (53%) and **25** (22%); (c) 10% AcOH (aq), 65 °C, 68 h, quant.; (d) KOH, MeOH, rt, 3h, quant.

2.2. X-ray crystallographic studies on the diastereomeric hexols 9–11

Crystals of the isomeric hexols **9**–**11**, suitable for single crystal X-ray crystallography, were grown under ambient temperature and pressure from their solutions in deionized water by slow solvent evaporation technique. Details of the packing patterns in the polycyclitols **9**–**11**, as gleaned from an analysis of their respective crystal data, are discussed below.

*2.2.1. Crystal structure of the hexol **9**.* Crystal structure of the hexol **9** was solved and refined in the centrosymmetric monoclinic space group $P2_1/c$ (Z=4) (Fig. 4). A pair of hydrogen bonds, involving O3···O5 and O6···O2, describes a $R_2^2(10)$ H-bonding motif and links the hexol molecules to form zigzag chains along the *c*-axis.[15] These molecular chains, translated along the *b*-axis, are in turn connected to each other by two H-bonds [hydrogen bonding motif: $R_2^2(10)$], which engage two vicinal tertiary (O1 and O4) and two vicinal secondary (O5 and O6) hydroxy moieties. The resulting self-assembly consists of columnar architectures, which are further linked to one another along the *a*-axis by hydrogen bonds involving O2···O1 and O4···O5 (Fig. 5, Table 1).

*2.2.2. Crystal structure of the hexol **10**.* The hexol **10** packed in the centrosymmetric monoclinic space group $C2/c$ (Z=8) (Fig. 6). As would have been expected from the NMR studies, the 1,3-syndiaxial hydroxy groups participated in intramolecular O–H···O hydrogen bonding. Unlike its diastereomeric sibling **9**, molecules of the hexol **10** form zigzag molecular chains along the *c*-axis via the agency of an intermolecular hydrogen bond involving O3···O5. These molecular chains, translated along the *b*-axis, are in turn linked by a pair of intermolecular O–H···O hydrogen bonds (O2···O6 and O6···O4). The molecular sheets, thus formed, are in turn connected to one other by two pairs of hydrogen bonds that constitute either a $R_4^4(8)$ H-bonding cycle (O5···O3) or a $R_2^2(10)$ motif (O4···O1) (Fig. 7, Table 2).[15]

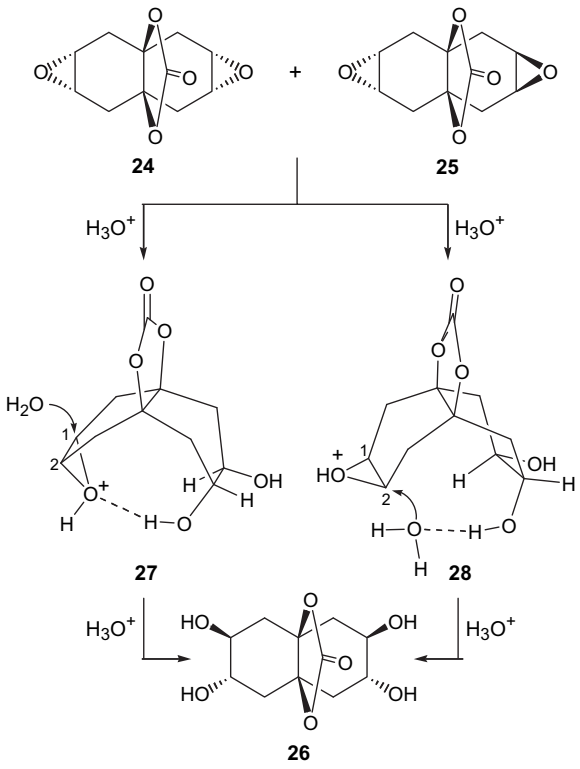

Scheme 3. Postulated mechanism for the observed stereo-convergence in the epoxide ring opening of the diepoxides **24** and **25**.

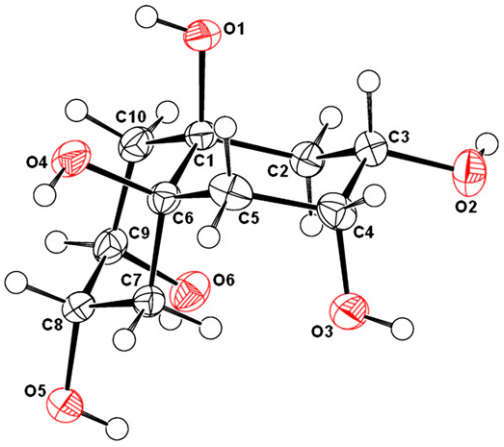

Fig. 4. ORTEP diagram of the hexol **9**, with the atom numbering scheme for the asymmetric unit. Displacement ellipsoids have been drawn at 50% probability level and H atoms are shown as small spheres of arbitrary radii.

*2.2.3. Crystal structure of the hexol **11**.* The hexol **11** underwent spontaneous resolution and crystallized in the chiral orthorhombic space group $P2_12_12_1$ (Z=8) with two molecules (A and B) of the hexol occupying the asymmetric unit (Fig. 8).[16,17] Isolation of the otherwise

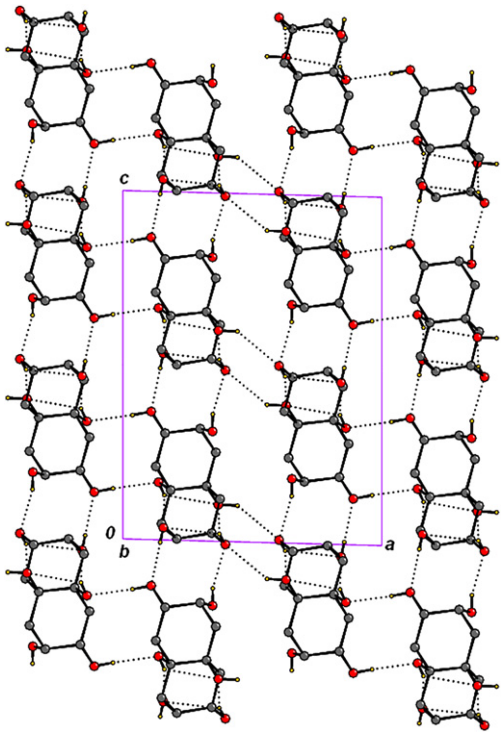

Fig. 5. Molecular packing in the hexol **9**. Dotted lines indicate the intermolecular O–H···O H-bonds. Hydrogen atoms bonded to carbon atoms have been omitted for the sake of clarity.

Table 1
Hydrogen bond geometry in the hexol **9**[a]

D–H···A	D–H (Å)	H···A (Å)	D···A (Å)	D–H···A (°)
O1–H1O···O6^{i}	0.82	2.04	2.829(2)	161
O2–H2O···O1^{ii}	0.82	1.98	2.796(2)	177
O3–H3O···O5^{iii}	0.82	2.00	2.778(2)	159
O4–H4O···O5^{iv}	0.82	2.42	3.103(2)	141
O5–H5O···O4^{v}	0.82	2.04	2.836(3)	162
O6–H6O···O2^{vi}	0.82	2.01	2.798(2)	161

[a] Symmetry codes: (i) $x, y-1, z$; (ii) $-x+2, y+1/2, -z+3/2$; (iii) $x, -y+3/2, z-1/2$; (iv) $-x+1, -y+1, -z+2$; (v) $x, y+1, z$; (vi) $x, -y+3/2, z+1/2$.

C_s symmetric **11** as a conglomerate supplemented the results of the NMR studies and pointed toward the fact that the hexol **11** exists as an enantiomeric mixture in solution on account of the strong intramolecular O–H···O H-bonding, which leads to a breakdown of the mirror symmetry in the molecule. Crystal structure analysis also confirmed that the 1,3-syndiaxial hydroxy groups in **11** do participate in intramolecular O–H···O H-bonding. Each of the two crystallographically independent molecules engages two vicinal tertiary [(O1 and O4) or (O7 and O10)] and two vicinal secondary [(O5 and O6) or (O11 and O12)] hydroxy moieties to form zigzag hydrogen bonded [H-bonding motif: $R_2^2(10)$] chains (alternating…AAA… and …BBB… types) growing parallel to the *b*-axis.[15] Intermolecular O–H···O H-bonds, involving O9···O5, O3···O11, and O2···O12, link these molecular chains to form sheets essentially perpendicular to the *a*-axis. The molecular sheets, translated along the *a*-axis, are further interconnected by hydrogen bonds, involving O8···O3, O4···O11, and O10···O6, to engender the intricate three-dimensional supramolecular assembly of the hexol **11** (Fig. 9, Table 3).

2.3. Comparison of the hydrogen bonded self-assemblies of the polycyclitols 9–11

Crystal structures of the three diastereomeric hexols **9**–**11** differ, like that observed for their conformationally locked siblings

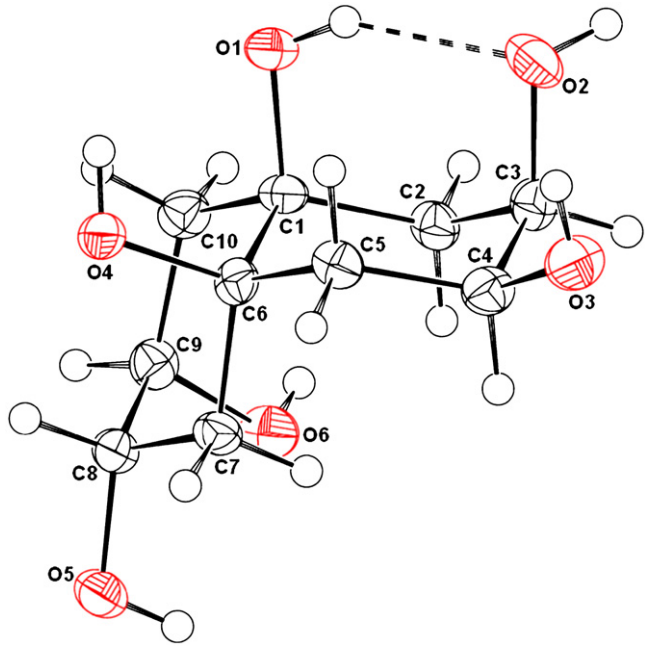

Fig. 6. ORTEP diagram of the hexol **10**, with the atom numbering scheme for the asymmetric unit. Displacement ellipsoids have been drawn at 50% probability level and H atoms are shown as small spheres of arbitrary radii. Dotted lines indicate the intramolecular O–H···O H-bond.

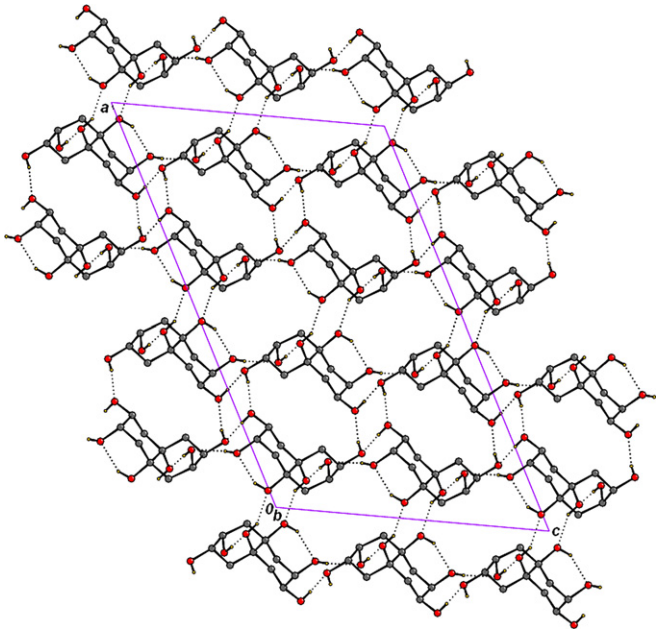

Fig. 7. Molecular packing in the hexol **10**. Dotted lines indicate the O–H···O H-bonds. Hydrogen atoms bonded to carbon atoms have been omitted for the sake of clarity.

1–**3**, in the number of nearest neighbors to which a hexol is hydrogen bonded and the number of H-bonds that the molecule forms (Table 4). However, as opposed to the individualistic nature of the crystal packing noted in case of **1**–**3**,[1d–f] an interesting similarity can be clearly discerned in the overall packing patterns of all three polycyclitols under study. A general description for the crystal packing in the hexols **9**–**11** would be: molecules form zigzag H-bonded chains, the translationally related chains link with one another to form sheets and the translationally related molecular

Table 2
Hydrogen bond geometry in the hexol **10**[a,b]

D–H···A	D–H (Å)	H···A (Å)	D···A (Å)	D–H···A (°)
O1–H1O···O2^{i}	0.82	1.95	2.688(3)	149
O2–H2O···O6^{ii}	0.82	2.08	2.886(3)	167
O3–H3O···O5^{iii}	0.82	1.98	2.775(3)	163
O4–H4O···O1^{iv}	0.82	2.04	2.772(3)	149
O5–H5O···O3^{v}	0.82	1.94	2.733(3)	164
O6–H6O···O4^{vi}	0.82	1.97	2.789(3)	173

[a] Symmetry codes: (i) x, y, z; (ii) $-x, -y+1, -z$; (iii) $x, -y+1, z+1/2$; (iv) $-x, -y+1, -z$; (v) $-x+1/2, y-1/2, -z+1/2$; (vi) $x, y-1, z$.
[b] Certain C–H···O hydrogen bonds, such as C3–H3A···O3 (d=2.54 Å, θ=152°), could also be discerned in the crystal structure of 10. However, these interactions resulted from the extensive O–H···O H-bonding, forcing the interacting atoms to approach nearer to each other.

sheets connect via hydrogen bonds to culminate in the observed crystal structure. A putative explanation for this commonality would lie probably in the ubiquitous presence of the $R_2^2(10)$ hydrogen bonding motif ('synthon') in the solid-state self-assemblies of **9**–**11**. It is pertinent to highlight at this point that the $R_2^2(10)$ dimer, which has been shown to be the preferred O–H···O hydrogen bonding motif in fully hydrogen bonded crystal structures of *vic*-diols,[18] has rarely been observed in the crystal structures of conformationally locked hexols **1**–**6**. This seems to be the key differentiator in the packing patterns of the *cis*- and the *trans*-decalin based hexols and can be reconciled in terms of the prohibitive spatial separation of the vicinal hydroxy groups in the latter.

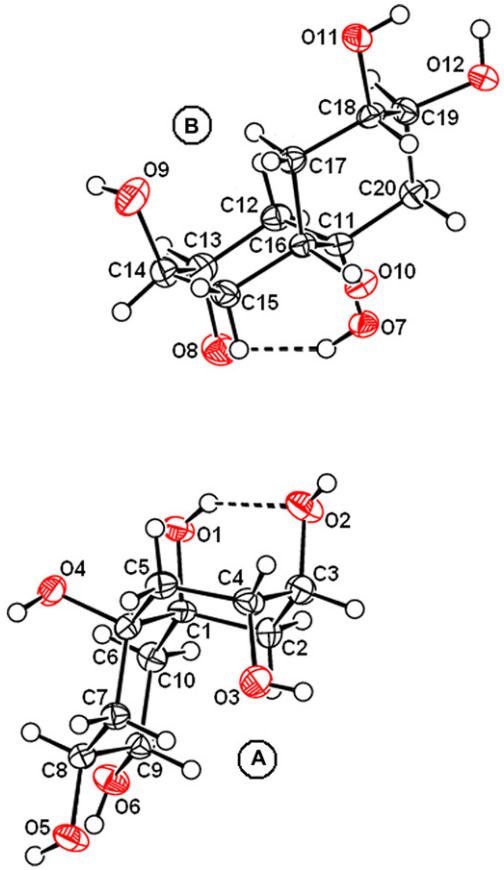

Fig. 8. ORTEP diagram of the hexol **11**, with the atom numbering scheme for the asymmetric unit. Displacement ellipsoids have been drawn at 50% probability level and H atoms are shown as small spheres of arbitrary radii. Dotted lines indicate the intramolecular O–H···O H-bonds.

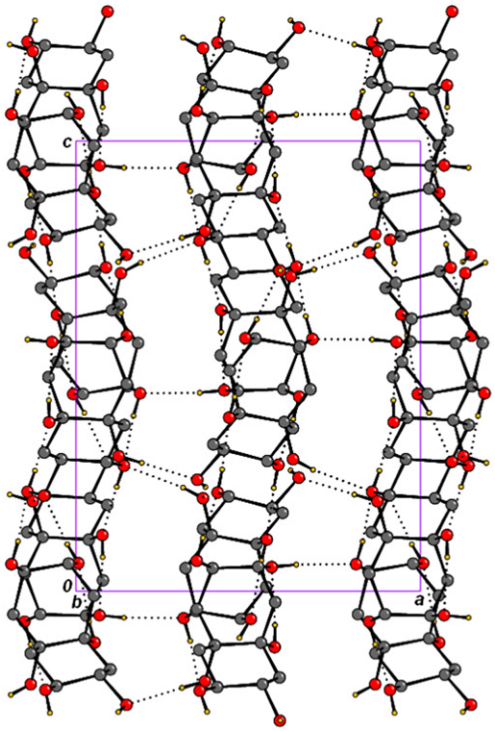

Fig. 9. Molecular packing in the hexol **11**. Dotted lines indicate the O–H···O H-bonds. Hydrogen atoms bonded to carbon atoms have been omitted for the sake of clarity.

Table 3
Hydrogen bond geometry in the hexol **11**[a,b]

D–H···A	D–H (Å)	H···A (Å)	D···A (Å)	D–H···A (°)
O1–H1O···O2^{i}	0.82	2.00	2.711(2)	145
O2–H2O···O12^{ii}	0.82	1.91	2.720(2)	171
O3–H3O···O11^{iii}	0.82	2.01	2.801(2)	162
O4–H4O···O11^{iv}	0.82	2.22	3.032(2)	171
O5–H5O···O1^{iv}	0.82	1.87	2.686(2)	176
O6–H6O···O4^{iv}	0.82	2.10	2.874(2)	157
O7–H7O···O8^{i}	0.82	1.95	2.687(2)	150
O8–H8O···O3^{v}	0.82	2.01	2.822(3)	173
O9–H9O···O5^{vi}	0.82	1.93	2.725(3)	162
O10–H10O···O6^{vii}	0.82	1.94	2.757(2)	172
O11–H11O···O7^{viii}	0.82	1.90	2.719(2)	176
O12–H12O···O10^{viii}	0.82	1.86	2.671(2)	168

[a] Symmetry codes: (i) x, y, z; (ii) $-x+3/2, -y+1, z-1/2$; (iii) $x-1/2, -y+3/2, -z$; (iv) $-x+1, y+1/2, -z+1/2$; (v) $x+1, y-1, z$; (vi) $x+1/2, -y+3/2, -z$; (vii) $x, y-1, z$; (viii) $-x+2, y+1/2, -z+1/2$.
[b] Certain C–H···O hydrogen bonds, such as C7–H7B···O7 (d=2.46 Å, θ=155°), could also be discerned in the crystal structure of **11**. However, these interactions resulted from the extensive O–H···O H-bonding, forcing the interacting atoms to approach nearer to each other.

Table 4
Characteristics of close packing in crystal structures of the hexols **9**–**11**.

	9	**10**	**11**
Number of nearest H-bonded neighbors	8	9	7
Number of intermolecular O–H···O hydrogen bonds per hexol molecule	12	10	10
Packing index	75.6%	71.1%	73.3%

3. Conclusions

In summary, our synthetic approach to *cis*-fused polycyclitols has revealed some interesting diastereoselections and stereo-convergences during the varied oxyfunctionalization protocols on a *cis*-

decalin framework. The results also highlight the role of intramolecular O–H···O hydrogen bonding in restraining the conformational flexibility of polyhydroxylated *cis*-decalins. The ubiquitous presence of the $R_2^2(10)$ dimer synthon as a robust O–H···O hydrogen bonding motif in polyhydroxylated *cis*-decalins is a noteworthy variation and marks a credible point of departure from the patterns of H-bonding identified for *trans*-decalin based polycyclitols.

4. Experimental section

4.1. Synthesis of the acetonide 17

A solution of the diol **16** (95 mg, 0.572 mmol) in dry acetone (10 mL) was stirred with Amberlyst-15 (~10 mg) and powdered type 4 Å molecular sieves (~30 mg) at room temperature for 1 h. The reaction mixture was filtered through a Celite pad and the filtrate concentrated under reduced pressure to give a residue, which, on chromatography over a silica gel column (10% ethyl acetate/petroleum ether), furnished the acetonide **17** (115 mg, 98%) as a colorless liquid. IR (neat) $\bar{\nu}_{max}$=3025, 2841, 1645, 1429, 1377, 1211 cm^{-1}; ^1H NMR (400 MHz, $CDCl_3$, 298 K) δ 5.70 (s, 2H), 4.38–4.36 (m, 2H), 2.63 (s, 4H), 2.16–2.14 (m, 4H), 1.40 (s, 3H), 1.33 (s, 3H); ^{13}C NMR (100 MHz, $CDCl_3$, 298 K) δ 124.5 (2C), 124.1 (2C), 107.7, 73.7 (2C), 33.2 (2C), 31.5 (2C), 27.2, 25.1; Mass (EI, 70 eV) *m*/*z* 206 [M^+].

4.2. Synthesis of the bisacetonides 19 and 20

To a solution of the acetonide **17** (89 mg, 0.432 mmol) in 2 mL of 4:1 acetone/water mixture, a catalytic amount of solid osmium tetroxide (11 mg, 10 mol %), followed by 50 wt % solution of NMMO in water (0.200 mL, 0.101 mmol), was added. The resulting solution was allowed to stir at ambient temperature for 48 h, after which the reaction was quenched by the addition of solid sodium sulfite (600 mg). The mixture was then diluted with acetone to precipitate the inorganic salts and filtered through a short pad of Celite. After washing the filter bed thoroughly with acetone, the combined filtrate and washings were concentrated under reduced pressure to obtain the tetrol **18** as a mixture of two diastereomers (as indicated by TLC). The latter was put directly for acetonide protection without any further purification.

The crude tetrol **18**, obtained in the previous step, was dissolved in dry acetone (4 mL) and allowed to react with 2,2-Dimethoxypropane (91 mg, 0.110 mL, 0.874 mmol) in presence of PPTS (12 mg, 0.043 mmol) for 2 h. The volatiles were then removed under vacuum and chromatographic separation of the resultant residue over silica gel with 40% ethyl acetate/petroleum ether yielded successively **20** (63 mg, 45%) and **19** (60 mg, 44%) in 89% combined yield (over two steps).

Bisacetonide **19**: Mp 268–269 °C; IR (thin film) $\bar{\nu}_{max}$=3450, 2929, 1599, 1431, 1248, 1134 cm^{-1}; ^1H NMR (400 MHz, DMSO-d_6, 298 K) δ 4.18 (s, 2H), 4.16 (dd appearing as a t, *J*=4 Hz, 4H), 1.87 (d, *J*=6 Hz, 8H), 1.36 (s, 6H), 1.19 (s, 6H); ^{13}C NMR (100 MHz, DMSO-d_6, 298 K) δ 106.9 (2C), 72.8 (4C), 71.4 (2C), 38.4 (4C), 28.3 (2C), 25.9 (2C); HRMS (ES) *m*/*z* calcd for $C_{16}H_{26}O_6Na$ $(M+Na)^+$: 337.1627; found: 337.1626.

Bisacetonide **20**: Mp 157–158 °C; IR (thin film) $\bar{\nu}_{max}$=3492, 2985, 2931, 1599, 1381, 1244, 1218, 1022 cm^{-1}; ^1H NMR (400 MHz, $CDCl_3$, 298 K) δ 4.35 (dd appearing as a t, *J*=4 Hz, 2H), 4.21 (dd appearing as a t, *J*=4 Hz, 2H), 3.04 (s, 2H), 2.26 (dd, *J*=15, 5 Hz, 2H), 2.09 (dd, *J*=15, 5 Hz, 2H), 2.06 (dd, *J*=15, 5 Hz, 2H), 1.74 (dd, *J*=15, 4 Hz, 2H), 1.53 (s, 3H), 1.45 (s, 3H), 1.33 (s, 3H), 1.32 (s, 3H); ^{13}C NMR (100 MHz, $CDCl_3$, 298 K) δ 108.5, 108.0, 73.3 (2C), 73.1 (2C), 72.3 (2C), 37.4 (2C), 35.4 (2C), 28.8. 28.6, 26.1, 26.0; HRMS (ES) *m*/*z* calcd for $C_{16}H_{26}O_6Na$ $(M+Na)^+$: 337.1627; found: 337.1626.

4.3. Synthesis of the hexols 9 and 10

The bisacetonide **19** (13 mg, 0.041 mmol) was warmed at 60 °C for 1 h with 10% v/v aqueous acetic acid (2 mL). The volatiles were removed completely under vacuum to obtain the pure hexol **9** (10 mg) as colorless solid in quantitative yield. Mp 246–247 °C (decomp.); IR (KBr) $\bar{\nu}_{max}$=3390, 3270, 2910, 1451, 1078, 1060, 1041, 1023, 877, 731 cm^{-1}; ^1H NMR (400 MHz, D_2O, 298 K) δ 3.76 (s, 4H), 2.30 (br s, 2H), 1.71 (br s, 2H), 1.53 (br s, 2H), 1.35 (br s, 2H); ^{13}C NMR (100 MHz, D_2O, 298 K) δ 73.6 (2C), 69.1 (2C), 67.5 (2C), 40.3 (2C), 38.2 (2C); ^1H NMR (400 MHz, D_2O, 343 K) δ 4.46 (dd appearing as a t, *J*=4 Hz, 4H), 2.61 (br s, 4H), 2.25 (d, *J*=14 Hz, 4H); ^{13}C NMR (100 MHz, D_2O, 343 K) δ 73.8 (2C), 68.6 (4C), 39.7 (4C); HRMS (ES) *m*/*z* calcd for $C_{10}H_{18}O_6Na$ $(M+Na)^+$: 257.1001; found: 257.1003.

Acetonide deprotection in **20** was carried out in an identical manner and afforded quantitatively the hexol **10**. Mp 272–274 °C (decomp.); IR (KBr) $\bar{\nu}_{max}$=3697, 2890, 1461, 1288, 1155, 1064, 1021, 1008, 741 cm^{-1}; ^1H NMR (400 MHz, D_2O, 298 K) δ 3.82–3.74 (m, 3H), 3.59 (d, *J*=12 Hz, 1H), 2.19 (d, *J*=16 Hz, 1H), 1.80 (dd appearing as a t, *J*=13 Hz, 1H), 1.74 (dd appearing as a t, *J*=13 Hz, 1H), 1.68–1.62 (m, 2H), 1.53 (d, *J*=15 Hz, 1H), 1.40 (m, 2H); ^{13}C NMR (100 MHz, D_2O, 298 K) δ 74.9, 73.2, 70.1, 68.9, 68.7, 67.1, 38.7, 38.6, 38.1, 35.8; ^1H NMR (400 MHz, D_2O, 353 K) δ 4.53 (dd appearing as a t, *J*=4 Hz, 2H), 4.39 (br s, 2H), 2.49–2.27 (series of m, 8H); ^{13}C NMR (100 MHz, D_2O, 353 K) δ 74.4 (2C), 70.0 (2C), 68.9 (2C), 38.9 (2C), 36.7 (2C); HRMS (ES) *m*/*z* calcd for $C_{10}H_{18}O_6Na$ $(M+Na)^+$: 257.1001; found: 257.1006.

4.4. Synthesis of the carbonate 23

Pyridine (142 mg, 0.146 mL, 1.800 mmol) and DMAP (4 mg, 10 mol %) were added to a solution of the diol **22** (50 mg, 0.301 mmol) in dry dichloromethane (1 mL) at ambient temperature. The resulting mixture was then cooled to −78 °C and a solution of triphosgene (45 mg, 0.150 mmol) in dry dichloromethane (1 mL) was added slowly for about 20 min with stirring. The reaction was subsequently allowed to proceed at ambient temperature for 2 h, after which it was quenched with saturated ammonium chloride solution and the product extracted with dichloromethane (3×30 mL). The combined extracts were washed successively with 1 N HCl, saturated sodium bicarbonate solution and brine, and finally dried over anhydrous sodium sulfate. Removal of the solvent and subsequent column chromatography over silica gel with 20% ethyl acetate/petroleum ether afforded the carbonate **23** (46 mg, 80%) as a colorless, crystalline solid. Mp 218–219 °C; IR (KBr) $\bar{\nu}_{max}$=3059, 2961, 2954, 1778, 1748, 1435, 1334, 1212, 1049, 703 cm^{-1}; ^1H NMR (400 MHz, $CDCl_3$, 298 K) δ 5.97 (dd appearing as a t, *J*=3 Hz, 4H), 2.63 (ddd, *J*=14, 4, 2 Hz, 4H), 2.21 (d, *J*=15 Hz, 4H); ^{13}C NMR (100 MHz, $CDCl_3$, 298 K) δ 154.5, 127.0 (4C), 87.0 (2C), 34.1 (4C); HRMS (ES) *m*/*z* calcd for $C_{11}H_{12}O_3Na$ $(M+Na)^+$: 215.2042; found: 215.2039.

4.5. Synthesis of the diepoxides 24 and 25

*m*CPBA (70% purity, 256 mg, 1.040 mmol) was added to a solution of the carbonate **23** (100 mg, 0.520 mmol) in dichloromethane (5 mL) at ambient temperature. The reaction was allowed to stir at room temperature for 2 days and then quenched by addition of a saturated solution of sodium sulfite in water. The product was extracted with dichloromethane (5×30 mL); the combined extracts were washed successively with saturated sodium bicarbonate solution and brine, followed by drying over anhydrous sodium sulfate. Removal of the solvent and subsequent purification of the resultant residue by column chromatography with ethyl acetate afforded a diastereomeric mixture of the diepoxides **24** and **25** (85 mg, 75% combined yield) as a colorless solid. Though

dispensable for the next step, chromatographic separation of this diepoxide mixture (product ratio=7:3) allows isolation of the major **24** with 40% ethyl acetate/petroleum ether and subsequently, the minor **25** with ethyl acetate alone.

Diepoxide **24**: mp 198–199 °C; IR (KBr) $\bar{\nu}_{max}$=2361, 2339, 1780, 1485, 1186, 1146 cm^{-1}; ^1H NMR (400 MHz, $CDCl_3$, 298 K) δ 3.25 (dd appearing as a t, J=2 Hz, 4H), 2.50 (dd, J=16, 4 Hz, 4H), 1.99 (ddd, J=15, 3, 1 Hz, 4H) ppm; ^{13}C NMR (100 MHz, $CDCl_3$, 298 K) δ 152.1, 83.5 (2C), 47.7 (4C), 35.6 (4C); HRMS (ES) m/z calcd for $C_{11}H_{12}O_5Na$ $(M+Na)^+$: 247.0582; found: 247.0616.

Diepoxide **25**: mp 243–244 °C; IR (KBr) $\bar{\nu}_{max}$=2955, 1786, 1768, 1324, 1078, 1041, 812, 764 cm^{-1}; ^1H NMR (400 MHz, DMSO-d_6, 298 K) δ 3.24 (dd appearing as a t, J=2 Hz, 2H), 3.20 (dd appearing as a t, J=3 Hz, 2H), 2.45 (dd, J=15, 3 Hz, 2H), 2.34 (ddd appearing as a td, J=16, 2 Hz, 2H), 2.14 (d, J=16 Hz, 2H), 1.71 (dd, J=15, 4 Hz, 2H); ^{13}C NMR (100 MHz, DMSO-d_6, 298 K) δ 151.9, 81.4 (2C), 48.5 (2C), 46.5 (2C), 34.5 (2C), 31.8 (2C); HRMS (ES) m/z calcd for $C_{11}H_{12}O_5Na$ $(M+Na)^+$: 247.0582; found: 247.0585.

4.6. Synthesis of the tetrol 26

The mixture of diepoxides (18 mg, 0.080 mmol), obtained in the previous step, was suspended in acetic acid (10% solution in water, 2 mL) and stirred vigorously at 60 °C for 68 h. The reaction mixture was then dried under vacuum to obtain the tetrol **26** (20 mg) in near quantitative yield. Mp 239–240 °C; IR (KBr) $\bar{\nu}_{max}$=3298, 2454, 1782, 1214, 1064, 1030 cm^{-1}; ^1H NMR (400 MHz, D_2O, 298 K) δ 3.77–3.75 (m, 2H), 3.65–3.63 (m, 2H), 2.23–2.16 (m, 4H), 2.02–1.94 (m, 4H); ^{13}C NMR (100 MHz, D_2O, 298 K) δ 155.7, 85.7, 84.4, 68.7 (2C), 68.3 (2C), 36.6 (2C), 36.4 (2C); HRMS (ES) m/z calcd for $C_{11}H_{16}O_7Na$ $(M+Na)^+$: 283.0794; found:283.0805.

4.7. Synthesis of the hexol 11

The tetrol **26** (10 mg, 0.038 mmol) was taken up in 2 mL of dry methanol and stirred at ambient temperature with solid potassium hydroxide (4 mg, 0.079 mmol) for 3 h. The solvent was then removed completely under vacuum and the residue dissolved in minimum volume (0.8–1.0 mL) of deionized water. The aqueous solution was passed through a short column of pre-treated DOWEX®50 W ion-exchange resin (~1.5 g, 8–200 mesh, acidic cation) and washed with deionized water. The aqueous solution of the product thus obtained was concentrated under vacuum to obtain the hexol **11** (9 mg) in quantitative yield. Mp 251–252 °C (decomp.); IR (KBr) $\bar{\nu}_{max}$=3706, 3151, 2925, 1456, 1275, 1093, 1052, 1011, 877, 822 cm^{-1}; ^1H NMR (400 MHz, D_2O, 298 K) δ 4.49–4.46 (m, 2H), 4.32 (m, 2H), 2.64–2.48 (m, 5H), 2.46–2.34 (m, 3H); ^{13}C NMR (100 MHz, D_2O, 298 K) δ 74.7, 73.9, 73.1, 71.2, 71.0, 70.4, 41.2, 40.9, 39.6, 36.3; ^1H NMR (400 MHz, D_2O, 348 K) δ 4.36 (dd, J=12, 6 Hz, 2H), 4.20 (dd, J=11, 7 Hz, 2H), 2.53–2.44 (m, 6H), 2.32 (dd, J=14, 7 Hz, 2H); ^{13}C NMR (100 MHz, D_2O, 343 K) δ 75.2, 73.7, 71.4 (2C), 71.2 (2C), 39.3 (2C), 38.1 (2C); HRMS (ES) m/z calcd for $C_{10}H_{18}O_6Na$ $(M+Na)^+$: 257.1001; found: 257.1011.

4.8. Crystal structure analysis

Single crystal X-ray diffraction data (Table 5) was collected at 291 K on a Bruker AXS SMART APEX CCD diffractometer using graphite monochromated Mo Kα radiation (λ=0.71073 Å). The X-ray generator was operated at 50 kV and 40 mA. The data was collected with a ω scan width of 0.3°. A total of 606 frames per set were collected using *SMART*[19] in three different settings of φ (0°, 90°, and 180°). During data collection, the sample to detector distance and the 2θ value was kept fixed at 6.062 cm and −25°, respectively. The data were reduced by *SAINTPLUS*;[19] an empirical absorption correction was applied using the package *SADABS*,[20] and *XPREP*[19] was used to determine the space group. The crystal structures were solved by direct methods using *SIR92*[21] and refined by full-matrix least-squares methods on F^2 using *SHELXL97*.[22] Molecular and packing diagrams were generated using *ORTEP-3*[23] and *CAMERON*,[24] respectively. The geometric calculations were done by *PARST*[25] and *PLATON*.[26] All hydrogen atoms, including those of hydroxy groups, were placed in geometrically idealized positions and constrained to ride on their parent atoms with C–H distances in the range 0.97–0.98 Å and U_{iso}(H)=1.2U_{eq}(C), and O–H distances fixed at 0.82 Å and U_{iso}(H)=1.5U_{eq}(O). CCDC 796419 (hexol **9**), CCDC 796420 (hexol **10**), CCDC 796421 (hexol **11**), and CCDC 796422 (diepoxide **24**) contain the supplementary crystallographic data for this paper. These data can be obtained free of charge from The Cambridge Crystallographic Data Center via www.ccdc.cam.ac.uk/data_request/cif.

Table 5
Summary of crystal data, data collection, structure solution, and refinement details

	9	10	11
Formula	$C_{10}H_{18}O_6$	$C_{10}H_{18}O_6$	$C_{10}H_{18}O_6$
M_r	234.24	234.24	234.24
Crystal system	monoclinic	monoclinic	orthorhombic
Space group	$P2_1/c$	$C2/c$	$P2_12_12_1$
a [Å]	11.099(3)	24.154(14)	11.5049(8)
b [Å]	6.0796(15)	6.585(4)	11.9856(9)
c [Å]	14.970(4)	15.125(9)	15.0103(11)
α [°]	90	90	90
β [°]	91.505(4)	117.117(10)	90
γ [°]	90	90	90
V [Å^3]	1009.8(5)	2141(2)	2069.8(3)
Z	4	8	8
F (000)	504	1008	1008
ρ_{calcd} [g cm^{-3}]	1.541	1.453	1.503
μ [mm^{-1}]	0.127	0.120	0.124
Reflns collected	7144	7552	15,567
l.s. parameters	151	151	301
Unique reflns	1870	1975	2193
Observed reflns	1385	1598	2085
R_1 [$I>2\sigma(I)$]	0.0500	0.0453	0.0330
wR_2 [$I>2\sigma(I)$]	0.1033	0.1188	0.0814
Goodness of fit	1.090	0.884	1.074
$\Delta\rho_{max/min}$ [e Å^{-3}]	0.300/−0.188	0.198/−0.233	0.229/−0.195

Acknowledgements

Part of the work described here was carried out at the Indian Institute of Science (IISc), Bangalore. S.S. and T.H.S. thank UGC and CSIR for support through a Dr. D.S. Kothari Post-doctoral fellowship and Research Associateship, respectively. G.M. wishes to thank Eli Lilly and Jubilant Bhartia Foundation for the current research support and the Government of India for the award of National Research Professorship.

Supplementary data

Supplementary data scanned copies of ^1H and ^{13}C NMR spectra of all new compounds have been provided. Supplementary data related to this article can be found online at doi:10.1016/j.tet.2011.03.042. These data include MOL files and InChIKeys of the most important compounds described in this article.

References and notes

1. (a) Mehta, G.; Sen, S.; Venkatesan, K. *CrystEngComm* **2005**, *7*, 398–401; (b) Mehta, G.; Sen, S.; Ramesh, S. S. *CrystEngComm* **2005**, *7*, 563–568; (c) Mehta, G.; Sen, S. *CrystEngComm* **2005**, *7*, 656–663; (d) Mehta, G.; Sen, S.; Ramesh, S. S. *Eur. J. Org. Chem.* **2007**, 423–436; (e) Mehta, G.; Sen, S.; Venkatesan, K. *CrystEngComm* **2007**, *9*, 144–151; (f) Mehta, G.; Sen, S. *Eur. J. Org. Chem.* **2009**, 123–131; (g) Mehta, G.; Sen, S. *Chem. Commun.* **2009**, 5981–5983; (h) Mehta, G.; Sen, S. *Tetrahedron* **2009**, *65*, 9713–9718; (i) Mehta, G.; Sen, S. *Tetrahedron Lett.* **2010**, *51*, 503–507; (j) Mehta, G.; Sen, S. *Acta Crystallogr., Sect. C: Cryst.*

Struct. Commun. **2010**, *66*, o59–o63; (k) Mehta, G.; Sen, S. *Eur. J. Org. Chem.* **2010**, 3387–3394; (l) Mehta, G.; Sen, S. *J. Org. Chem.* **2010**, *75*, 8287–8290.

2. (a) Mehta, G.; Ramesh, S. S.; Bera, M. K. *Chem.—Eur. J.* **2003**, *9*, 2264–2272; (b) Mehta, G.; Ramesh, S. S. *Tetrahedron Lett.* **2003**, *44*, 3105–3108; (c) Mehta, G.; Ramesh, S. S. *Eur. J. Org. Chem.* **2005**, 2225–2238.
3. (a) Jeffrey, G. A.; Saenger, W. *Hydrogen Bonding in Biological Structures*; Springer: Berlin, 1991; (b) Jeffrey, G. A. *An Introduction to Hydrogen Bonding*; Oxford University: Oxford, UK, 1997; (c) Jeffrey, G. A. *Acta Crystallogr., Sect. B: Struct. Sci.* **1990**, *46*, 89–103; (d) Jeffrey, G. A. *Crystallogr. Rev.* **2003**, *9*, 135–176.
4. (a) Mehta, G.; Ramesh, S. S. *Chem. Commun.* **2000**, 2429–2430; (b) Mehta, G.; Ramesh, S. S. *Tetrahedron Lett.* **2001**, *42*, 1987–1990; (c) Mehta, G.; Ramesh, S. S. *Can. J. Chem.* **2005**, *83*, 581–594.
5. (a) Kroon-Batenburg, L. M. J.; Kanters, J. A. *Acta Crystallogr., Sect. B: Struct. Sci.* **1983**, *39*, 749–754; (b) Gellman, S. H.; Dado, G. P.; Liang, C.-B.; Adam, B. R. *J. Am. Chem. Soc.* **1991**, *113*, 1164–1173; (c) Brady, J. W.; Schmidt, R. K. *J. Phys. Chem.* **1993**, *97*, 958–966; (d) Velde, D. G. V.; Georg, G. I.; Grunewald, G. L.; Gunn, C. W.; Mitscher, L. A. *J. Am. Chem. Soc.* **1993**, *115*, 11650–11651; (e) Yasuda, T.; Ikawa, S.-I. *J. Chem. Soc., Faraday Trans.* **1997**, *93*, 1869–1874; (f) Robertson, E. G.; Simons, J. P. *Phys. Chem. Chem. Phys.* **2001**, *3*, 1–18; (g) Nangia, A. *Acc. Chem. Res.* **2008**, *41*, 595–604; (h) Takahashi, O.; Kohno, Y.; Nishio, M. *Chem. Rev.* **2010**, *110*, 6049–6076.
6. An in-depth study into the energetics of intramolecular O–H···O hydrogen bonding *vis-à-vis* solvation in hydroxyethers, modelled on a cis-perhydrochromene framework, has been reported by Beeson, et al. See: Beeson, C.; Pham, N.; Shipps, G., Jr.; Dix, T. A. *J. Am. Chem. Soc.* **1993**, *115*, 6803–6812.
7. In a cognate approach, amino acids, constructed on a *cis*-decalin scaffold, have been employed as conformation-based probes for investigating the effect of solvent on the energetics of intramolecular ion pairs (salt bridges between ammonium and carboxylate ions, in particular). See: (a) Beeson, C.; Dix, T. A. *J. Org. Chem.* **1992**, *57*, 4386–4394; (b) Beeson, C.; Dix, T. A. *J. Am. Chem. Soc.* **1993**, *115*, 10275–10281.
8. The synthesis and characterization of the acetonide **17** have been reported in the thesis dissertation of Dr. Senaiar S. Ramesh, Indian Institute of Science, Bangalore, India, 2004.
9. For references discussing the influence of solvation and water bridges on molecular conformation, see: (a) Tayar, N. E.; Mark, A. E.; Vallat, P.; Brunne, R. M.; Testa, B.; van Gunsteren, W. F. *J. Med. Chem.* **1993**, *36*, 3757–3764; (b) Engelsen, S. B.; Pérez, S. *Carbohydr. Res.* **1996**, *292*, 21–38; (c) Cammers-Goodwin, A.; Allen, T. J.; Oslick, S. L.; McClure, K. F.; Lee, J. H.; Kemp, D. S. *J. Am. Chem. Soc.* **1996**, *118*, 3082–3090; (d) Takano, K.; Funahashi, J.; Yamagata, Y.; Fujii, S.; Yutani, K. *J. Mol. Biol.* **1997**, *274*, 132–142; (e) Oesterhelt, F.; Rief, M.; Gaub, H. E. *New J. Phys.* **1999**, *1*, 6.1–6.11; (f) Poon, C.-D.; Samulski, E. T.; Weise, C. F.; Weisshaar, J. C. *J. Am. Chem. Soc.* **2000**, *122*, 5642–5643; (g) Kirschner, K. N.; Woods, R. J. *Proc. Natl. Acad. Sci. U.S.A.* **2001**, *98*, 10541–10545; (h) Carney, J. R.; Dian, B. C.; Florio, G. M.; Zwier, T. S. *J. Am. Chem. Soc.* **2001**, *123*, 5596–5597; (i) Zwier, T. S. *J. Phys. Chem. A* **2001**, *105*, 8827–8839; (j) Drozdov, A. N.; Grossfield, A.; Pappu, R. V. *J. Am. Chem. Soc.* **2004**, *126*, 2574–2581; (k) Zwier, T. S. *J. Phys. Chem. A* **2006**, *110*, 4133–4150; (l) Barnett, C. B.; Naidoo, K. J. *J. Phys. Chem. B* **2008**, *112*, 15450–15459.
10. For references pertinent to intramolecular hydrogen bonding, limiting the conformational flexibility of a molecule in solution, see: (a) Higuchi, S.; Kikugawa, K. *Nucleic Acids Res.* **1978**, *1*, s367–s372; (b) Glusker, J. P.; Zacharias, D. E.; Whalen, D. L.; Friedman, S.; Pohl, T. M. *Science* **1982**, *215*, 695–696; (c) Liang, G.-B.; Dado, G. P.; Gellman, S. H. *J. Am. Chem. Soc.* **1991**, *113*, 3994–3995; (d) Holmbeck, S. M. A.; Petillo, P. A.; Lerner, L. E. *Biochemistry* **1994**, *33*, 14246–14255; (e) Dais, P.; Tylianakis, E.; Kanetakis, J.; Taravel, F. R. *Biomacromolecules* **2005**, *6*, 1397–1404; (f) Ahn, H. C.; Choi, K. *Org. Lett.* **2007**, *9*, 3853–3855; (g) Lerbret, A.; Mason, P. E.; Venable, R. M.; Cesàro, A.; Sabougni, M.-L.; Pastor, R. W.; Brady, J. W. *Carbohydr. Res.* **2009**, *344*, 2229–2235; (h) Gandhi, V. B.; Luo, Y.; Liu, X.; Shi, Y.; Klinghofer, V.; Johnson, E. F.; Park, C.; Giranda, V. L.; Penning, T. D.; Zhu, G.-D. *Bioorg. Med. Chem. Lett.* **2010**, *20*, 1023–1026; (i) Ogoshi, T.; Kitajima, K.; Aoki, T.; Yamagishi, T.-a.; Nakamoto, Y. *J. Phys. Chem. Lett.* **2010**, *1*, 817–821.
11. The molecular electrostatic potential surface (MEPS) diagrams were generated using MDL® Chime, Version 2.6 SP6.
12. Ashkenazi, P.; Kalo, J.; Rüttimann, A.; Ginsberg, D. *Tetrahedron* **1978**, *34*, 2161–2165.
13. **Crystal data for the diepoxide 24**. $C_{11}H_{12}O_5$, M=224.21, orthorhombic, *P*bcn, a=11.264(3), b=7.583(2), c=11.680(3) Å, V=997.6(5) Å^3, Z=4, ρ_{calcd}=1.493 g/cm^3, 6714 reflections measured, 922 unique (R_{int}=0.0447), $R1$=0.0496 and w$R2$=0.0960 for 668 observed reflections. An ORTEP diagram of **24**, with displacement ellipsoids for non-H atoms drawn at 50% probability level, has been shown below.

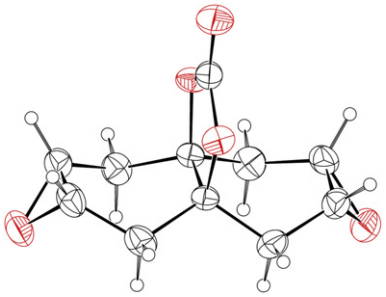

14. For selected references on the hydrogen bonding assisted nucleophillic ring opening of epoxides, see: (a) Kupchan, S. M.; Schubert, R. M. *Science* **1974**, *185*, 791–793; (b) Dalzell, H. C.; Razdan, R. K.; Sawdaye, R. *J. Org. Chem.* **1976**, *41*, 1650–1652; (c) Janusz, J. M.; Becker, A. R.; Bruice, T. C. *J. Am. Chem. Soc.* **1978**, *100*, 8269–8271; (d) Pihko, P. M. *Hydrogen Bonding in Organic Synthesis*; Wiley-VCH: 2009.
15. (a) Etter, M. C. *Acc. Chem. Res.* **1990**, *23*, 120–126; (b) Etter, M. C.; MacDonald, J. C.; Berstein, J. *Acta Crystallogr., Sect. B: Struct. Sci.* **1990**, *46*, 256–262; (c) Bernstein, J.; Davis, R. E.; Shimoni, L.; Chang, N.-L. *Angew. Chem., Int. Ed. Engl.* **1995**, *34*, 1555–1573.
16. Due to the absence of any significant anomalous scatterers (Z>Si) in **11**, attempts to confirm its absolute structure by refinement of the Flack parameter led to inconclusive results (see Ref. 17). Therefore the intensities of the Friedel pairs (1652) were averaged prior to merging of data in $P2_12_12_1$ and the absolute configuration was assigned arbitrarily. The reported value of R_{int} corresponds to subsequent merging of equivalent reflections in this space group.
17. (a) Flack, H. D. *Acta Crystallogr., Sect. A: Found. Crystallogr.* **1983**, *39*, 876–888; (b) Flack, H. D.; Bernardinelli, G. *J. Appl. Crystallogr.* **2000**, *33*, 1143–1148.
18. Brock, C. P. *Acta Crystallogr., Sect. B: Struct. Sci.* **2002**, *58*, 1025–1031.
19. *Bruker. SMART (Version 6.028), SAINT (Version 6.02), XPREP*; Bruker AXS: Madison, Wisconsin, USA, 1998.
20. Sheldrick, G. M. *SADABS (Version 2.10)*; University of Göttingen: Germany, 2003.
21. Altomare, A.; Cascarano, G.; Giacovazzo, C.; Guagliardi, A.; Burla, M. C.; Polidori, G.; Camalli, M. *J. Appl. Crystallogr.* **1994**, *27*, 435.
22. Sheldrick, G. M. *Acta Crystallogr., Sect. A: Found. Crystallogr.* **2008**, *64*, 112–122.
23. Farrugia, L. J. *J. Appl. Crystallogr.* **1997**, *30*, 565.
24. Watkin, D. M.; Pearce, L.; Prout, C. K. *CAMERON—A Molecular Graphics Package*; Chemical Crystallography Laboratory, University of Oxford: Oxford, UK, 1993.
25. Nardelli, M. *J. Appl. Crystallogr.* **1995**, *28*, 659.
26. Spek, A. L. *J. Appl. Crystallogr.* **2003**, *36*, 7–13.